Journal of Organometallic Chemistry 838 (2017) 12–23

Contents lists available at ScienceDirect

Journal of Organometallic Chemistry

journal homepage: www.elsevier.com/locate/jorganchem

Caenorhabditis elegans as a model for exploring the efficacy of synthesized organoruthenium complexes for aging and *Alzheimer's* disease a neurodegenerative disorder: A systematic approach

G. Devagi [a], G. Shanmugam [b], A. Mohankumar [b], P. Sundararaj [b, *], F. Dallemer [c], P. Kalaivani [d], R. Prabhakaran [a, *]

[a] Department of Chemistry, Bharathiar University, Coimbatore 641 046, India
[b] Department of Zoology, Bharathiar University, Coimbatore 641 046, India
[c] Laboratoire MADIREL CNRS UMR7246, Université of Aix-Marseille, Centre de Saint-Jérôme, bât. MADIREL, 13397 Marseille cedex 20, France
[d] Department of Chemistry, Nirmala College for Women, Bharathiar University, Coimbatore 641018, India

ARTICLE INFO

Article history:
Received 6 January 2017
Received in revised form
8 March 2017
Accepted 9 March 2017
Available online 14 March 2017

Keywords:
Ruthenium(II) complexes
Spectroscopy
X-ray crystallography
CT-DNA/ BSA protein binding
Anti-oxidant activity
C. elegans
Toxicology
ROS
Alzheimer's diseases

ABSTRACT

The current article deals with the preparation and characterisation of new organoruthenium(II) complexes, namely [RuCp(Dea-Sal-tsc)(PPh_3)] (**1**), [RuCp(Dea-Sal-mtsc)(PPh_3)] (**2**), [RuCp(Dea-Sal-etsc)(PPh_3)] (**3**) and [RuCp(Dea-Sal-ptsc)(PPh_3)] (**4**). The new ruthenium(II) complexes were characterized by various analytical, spectral techniques. The structure of the ligand [H_2-Dea-Sal-tsc] and the complex [RuCp(Dea-Sal-tsc)(PPh_3)] (**1**) were confirmed by X-ray crystallography. The complexes (**1**–**4**) were used to study the toxicity, stress resistance, aging and neuro-protective effects by taking *Caenorhabditis elegans* as model. *In vitro* free radical scavenging activity was performed by DPPH free radical scavenging assay, the complexes (**1**–**4**) exhibited highest scavenging activity than standard Vitamin C ($IC_{50} = 5.28 \pm 0.10$). The lifespan has increased over 22.4% in *mev-1* mutant worms treated with complex **4**. The complex **4** triggered the DAF-16 nuclear localization, increases *sod-3* expression and reduced amyloid ($A\beta$) protein induced paralysis were observed. In the present study we confirmed that oxidative stress resistance of N2 and lifespan extension of *mev-1* mutant which showed the potential ROS scavenging activity of complex **4**. The results also confirmed the effective anti-aging potential of ruthenium complex **4** which may be developed as a therapeutic drug for the prevention of aging and age related neurodegenerative diseases. Further studies are required to find out the exact action of complex **4** on higher model.

1. Introduction

Aging study, with specific attention on solving the underlying mechanisms of longevity, is becoming increased scientific interest. Lifespan is influenced by genes controlling metabolic activity, antioxidant systems, DNA repair, cellular senescence, and cell death. Several lines of confirmation led to the broad acceptance that oxidative stress and inflammation are main determinants of the aging process [1–3]. Early, Harman [4] hypothesized in his free-radical theory of aging (FRTA) that aging results from the aggregation of molecular damage produced through by-products of the normal oxidative metabolism, called reactive oxygen species (ROS). The finding of the superoxide dismutase enzyme, which detoxifies the superoxide anion [5], additionally gave credibility to the free-radical theory of aging. The extent of ROS formation and oxidative damage to Mitochondrial DNA (mtDNA) is inversely correlated with longevity across species [6] also causes damage to cellular proteins, lipids, eventually contributing to various chronic diseases including cancer, diabetes, Parkinson's and Alzheimer's disease, cardiovascular disease and chronic inflammation [7].

If FRTA is correct, antioxidants should slow down aging and prolong lifespan by interfering directly in the generation of radicals or by scavenging them. Previously, Brown et al. showed that EGCG reduces ROS levels via DAF-16 dependent manner [8]. Many researchers have reported that a strong antioxidant, reduced the oxidative stress and extend the life span of wild-type *C. elegans*

* Corresponding authors.
E-mail addresses: sunpalan@gmail.com (P. Sundararaj), rpnchemist@gmail.com (R. Prabhakaran).

http://dx.doi.org/10.1016/j.jorganchem.2017.03.023
0022-328X/

[9–11]. ROS also play important physiological roles, including in cellular signaling pathways. For example, in mammals H_2O_2 is generated to strengthen insulin signaling by inactivating redox-sensitive signal-quenching phosphatases [12]. $O^{2-}$is also generated as an immune defense mechanism (the oxidative burst), which may also occur in invertebrate ssuch as *C. elegans* [13].

Alzheimer's disease (AD) is a main and incurable neurodegenerative disorder with a very high social influence [14]. Its etiopathogenesis is unclear, and no effective treatment is yet available even to slow down disease progression. The "amyloid cascade hypothesis" has encouraged to discover new drugs and methods to discover substances suitable of blocking amyloid protein aggregation and preventing its neurotoxicity and a lot of compounds with these properties were discovered in the past [15]. In this line, there are few platinum-phenanthroline based metallo drugs were prepared and investigated for their effectiveness in binding with Aβ 1–42, and blocking the aggregation by conferring an appreciable protection to cortical neurons [16].

Ruthenium compounds are, less toxic than platinum compounds; furthermore, ruthenium compounds showed a prominent reactivity toward histidines and selectively affect the conformation of Aβ (1–42), bearing three histidine residues in its N-terminal portion [17]. Daniela Valensin et al., reported that ruthenium(II) complex, fac-[$Ru(CO)_3Cl_2$-(N1-thz)] were (thz = 1,3-thiazole), forms a stable adduct with Aβ (1–28) however the ruthenium(II) centre is coordinated to histidines 13 and 14 simultaneously [18]. Messori et al., reported the promising *in vitro* anti-Alzheimer properties for a ruthenium(III) complex namely (PMRU20), showed to be highly effective in protecting cortical neurons against Aβ (1–42) toxicity, moreover PMRU20 is devoid of any significant toxicity *in vitro* at the applied concentrations, also it was neuroprotective even against the toxicity induced by Aβ 25–35 [19].

So far, the oxidative stress resistance and prolonged lifespan of *C. elegans* was investigated only for organic compounds. To the best of our knowledge, still now no one reported the oxidative stress and prolonged lifespan of *C. elegans* by organoruthenium complexes. Also only *in vitro* studies have been reported for metal complexes and metal ions on Alzheimer's diseases [19–22] and there is no report available on *in vivo* experimental implications for Alzheimer's disease based on organoruthenium complexes. Hence, we decided to study the impact of our newly synthesized organoruthenium complexes on *C. elegans* as model to reveal the aging and Alzheimer's disease.

The nematode *C. elegans* is an important animal model in various fields such as neurobiology and genetics. Work with *C. elegans* has led to seminal discoveries in the fields of neuroscience, development, cell death, signal transduction, RNA interference and aging [23]. Numerous physiological processes and stress responses that are noticed in higher organisms (e.g., humans) are preserved in *C. elegans*. According to bioinformatics approach, *C. elegans* homologues have been identified for 60–80% of human genes [24] and 12 out of 17 known signal transduction pathways are conserved in *C. elegans* and human [25].

Further, thiosemicarbazones are a class of Schiff base compounds showed different molecular geometry with metal complexes, and are familiar for their biological activity as antiparasitics, antibacterial, antifungal, antiviral and antitumoral agents [26].

Considering the above facts, we synthesized and characterized four new organoruthenium(II) complexes containing bio active thiosemicarbazones and investigated their impact on lifespan and Aβ toxicity of *C. elegans*. The complex **4** was found to have an excellent antioxidant activity also extend the life span of *mev-1* mutant strain compared to the rest of the complexes. In addition, we examined their effects on pathways regulated by the DAF-16/FOXO transcription factors. To confirm this a daf-16::GFP and sod-3p::GFP reporter constructs are used. Further, the neuroprotective effect of all complexes against Aβ toxic protein aggregation was examined.

2. Results and discussion

The reaction of [$RuCl(PPh_3)_2(\eta^5$-$C_5H_5)$] with an equimolar amount of various 4(*N*)-substituted thiosemicarbazones (H_2L^1 –H_2L^4) in methanol resulted in the formation of new complexes (Scheme. 1), the analytical data of which confirmed the stoichiometry of the complexes (**1**–**4**). The structure of the ligand (**H_2L^1**) and complex **1** were confirmed by X-ray crystallographic studies and attempts were made to grow single crystals of complex **2**–**4** in various organic solvents were unsuccessful. The complexes are soluble in common organic solvents such as dichloromethane, chloroform, benzene, acetonitrile, ethanol, methanol, dimethylformamide and dimethylsulfoxide.

2.1. Spectral investigation

The characteristic IR bands of the metal complexes (Fig. S1- S4) compared with that of the free ligands provide significant information regarding to the binding of the ligands to metal ions. In the IR spectra of the ligands, a broad band observed around 3407-3446 cm^{-1} corresponding to ν_{OH} was observed around 3404-3432 cm^{-1} in the complexes indicating the non-participation of phenolic oxygen in coordination [27]. A sharp band around 1631-1634 cm^{-1} in the ligands corresponding to $\nu_{C=N}$ azomethine group was shifted to lower frequency at 1501-1570 cm^{-1} in the complexes indicating the coordination of azomethine nitrogen to ruthenium atom [28]. A sharp band observed around 782-796 cm^{-1} corresponding to $\nu_{C=S}$ in the ligands was completely disappeared in the complexes and a new band appeared at 742-748 cm^{-1} has been assigned to $\nu_{C\text{-}S}$ indicating the enolisation of -NH–C=S and subsequent deprotonation prior to the coordination [29]. In addition, the characteristic absorption bands corresponding to the presence of triphenylphosphine are also found in the expected region around 1425, 1085, 695 cm^{-1} [30]. Electronic spectra of the new ruthenium(II) complexes were recorded in dichloromethane displayed two to three bands in the region 233–403 nm (Fig. S5). The bands at 233 nm have been assigned to the intra ligand transition which take place between the ligand orbitals [31]. However, the bands observed at 351–389 nm was notified to LMCT (s→d) [33]. The band observed at 403 nm in complex **4** was assigned to MLCT transition [32]. The ^{1}H-NMR spectra of the ligands and the complexes (Fig. S6- S21) have been recorded in DMSO/$CDCl_3$. The ligand showed a singlet at δ 11.04–11.40 ppm corresponding to phenolic –OH group. However, a singlet appeared at δ 11.61–11.62 ppm in the complexes indicates the non-participation of phenolic oxygen in coordination [35]. The remaining all other NMR descriptions are given in supporting information. The ^{13}C {^{1}H} NMR spectra of the complexes (**1**–**4**) contain resonances for the cyclopentadienyl ring carbons around δ 79.91–83.76 ppm [34]. The resonance observed around δ 160.44–169.14 ppm assigned to the azomethine (HC=N) carbon of the ligands [36]. Thiolic carbon signal of the ligand observed around δ 165.21–169.40 ppm [36]. The spectra also showed resonance in the range of δ 119.60–134.40 ppm for the aromatic carbons [36]. In all the complexes resonances observed around δ 40.48–47.38 ppm and δ 12.57–25.46 ppm were due to methylene and methyl carbons of diethylamino group of ligand. In complex **2** a signal observed at δ 39.89 ppm has been assigned to terminal HN–CH_3 carbons. In complex **3**, signals observed at δ 36.33 ppm and δ 18.86 ppm was corresponding to the presence of methylene and methyl carbons of ethyl group. In order to confirm the presence of triphenylphosphine, ^{31}P NMR spectra were

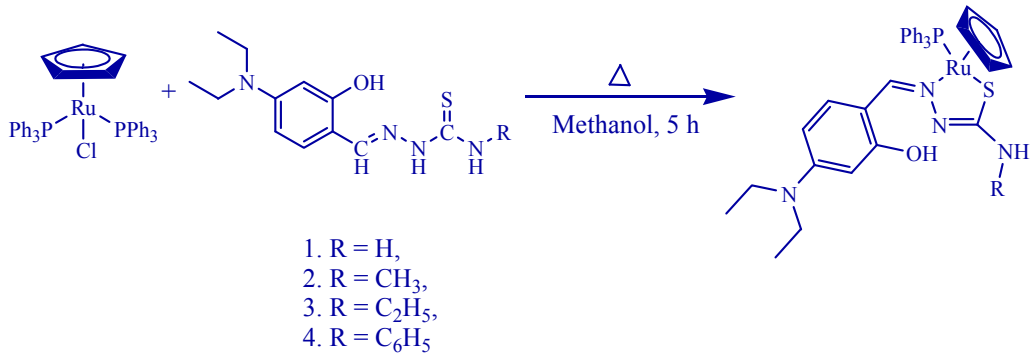

Scheme 1. Synthesis of new Ru(II) complexes.

recorded. The singlet observed at δ 29.28, 29.44, 29.36 and 29.40 ppm in complexes **1**, **2**, **3** and **4**, respectively, suggested the presence of a triphenylphosphine in each complexes [37].

2.2. Single crystal X-ray crystallography

The suitable crystals of $\mathbf{H_2L^1}$ and **1** suitable for X-ray diffraction studies were obtained from dichloromethane/*n*-hexane (1:1) mixture. The crystallographic data are listed in (Table 1**)**. The ORTEP diagrams of $\mathbf{H_2L^1}$ and **1** shown in (Figs. 1 and 2). In the ligand (H_2L^1), C(8)–S(1) bond, with the length of 1.6971(13) Å, is typical of double bonds; that is, the thioamide tautomer is present [38]. In complex, the ligand coordinated to ruthenium metal as NS chelating donor by forming a stable five member ring with a bite angle N(1)-Ru(1)-S(1) of 79.96(6)° and leaving the phenolic oxygen remains intact without involving in bonding. The Ru(1)–N(1) and Ru(1)–S(1) bond distances are found to be 2.096(2) Å and 2.3678 (9) Å respectively. The remaining sites are occupied by phosphorus atom of triphenylphosphine with Ru–P(1) distance of 2.2814 Å and five carbons of cyclopentadienyl ligand with Ru(1)–C(13), Ru(1)–C(14), Ru(1)–C(15), Ru(1)–C(16), Ru(1)–C(17) distance of 2.182 (4) Å, 2.205 (4) Å, 2.231 (3) Å, 2.183 (3) Å and 2.158 (4) Å respectively. The Ru(1)–S(1), Ru(1)–N(1) and Ru(1)–P(1) are comparable with the distances found in other octahedral ruthenium(II) complexes containing triphenylphosphine [39].

The selected bond distances and bond angles are given in (Table S1). The *cis* angles N(1)-Ru(1)-S(1) = 79.96(6)°, C(13)-Ru(1)-C(14) = 37.75(17)°, C(14)-Ru(1)-C(15) = 36.21(17)°, C(13)-Ru(1)-C(15) = 62.34(18)°, C(13)-Ru(1)-C(16) = 62.55(18)°, C(16)-Ru(1)-C(14) = 61.41(16)°, C(16)-Ru(1)-C(15) = 37.13(14)°, C(17)-Ru(1)-C(13) = 38.10(17)°, C(17)-Ru(1)-C(14) = 62.35(16)°, C(17)-Ru(1)-C(15) = 61.97(15)° and C(17)-Ru(1)-C(16) = 36.80(17)° are acute, whereas the other *cis* angles P(1)-Ru(1)-S(1) = 93.19(3)°, N(1)-Ru(1)-P(1) = 93.28(6)°, N(1)-Ru(1)-C(14) = 94.62(12)°, C(15)-Ru(1)-S(1) = 97.93(13)°,

C(16)-Ru(1)-S(1) = 98.71(14)° and C(17)-Ru(1)-P(1) = 92.75(11)° are obtuse. The *trans* angles are N(1)-Ru(1)-C(13) = 111.43(15)°, N(1)-Ru(1)-C(15) = 111.97(12)°, N(1)-Ru(1)-C(16) = 148.97(13)°, N(1)-Ru(1)-C(17) = 149.41(15)°, C(13)-Ru(1)-S(1) = 159.52(13)°, C(13)-Ru(1)-P(1) = 102.74(14)°, C(14)-Ru(1)-S(1) = 127.60(15)°, C(14)-Ru(1)-P(1) = 139.20(15)°, C(15)-Ru(1)-P(1) = 153.78(10)°, C(16)-Ru(1)-P(1) = 117.71(11)° and C(17)-Ru(1)-S(1) = 129.56(14)° were found similar to the reported values. The variations in bond lengths and angles lead to a significant distortion from an ideal octahedral geometry of the complex.

The ligand $\mathbf{H_2L^1}$ showed one intra and inter molecular hydrogen bonding through the hydrogen atom of the hydroxyl group with the hydrazinic nitrogen (N2) of thiosemicarbazone moiety with an O(1)–H(1)···N(1) distance of 2.721 Å and oxygen atom of hydroxyl group with the hydrogen atom of terminal nitrogen (N3) atom of another molecule with O(1)–H(1)···N(3) distance of 2.964 Å. Further, the complex **1** contains an intramolecular hydrogen bond (Table S2, Figs. S24 and S25) through the hydrogen atom of the hydroxyl group with the hydrazinic nitrogen (N2) of thiosemicarbazone moiety with O1–H(1)···N2 distance of 2.589 Å.

3. DNA binding studies

UV absorption titration experiments were carried out to study the DNA binding property of the new Ru(II) complexes (**1**–**4**). The absorption spectra of the new complexes at constant concentration (10 μM) in the presence of different concentration of CT-DNA (5–50 μM) are given in Fig. 3. The absorption spectra of complexes (**1**–**4**) mainly consist of two resolved bands [Intra ligand (IL) and CT transitions]. Intra ligand transitions of complexes **1**, **2**, **3** and **4** centered at 249 nm, 250 nm, 248 nm and 249 nm respectively. As the DNA concentration is increased, all the complexes (**1**–**4**) showed hyperchromism around (A = 0.1883–0.8562) with a red shift of 8 nm, 7 nm, 9 nm and 8 nm respectively. However, CT band of the complexes **1**–**4** were centered at 400 nm, 384 nm, 415 nm and 383 nm respectively. All the complexes showed hypochromism upon addition of CT-DNA around (A = 0.1671–0.1808) without any shift in the complexes (**1**–**3**) and 2 nm red shift in complex **4**. All the complexes exhibited isosbestic spectral change upon addition of CT-DNA to complexes (**1**–**4**) at 340 nm, 329 nm, 383 nm and 340 nm respectively. The observed hypochromic effect with or without shift in the charge transfer band suggested that the new ruthenium(II) complexes bind with adjacent base pairs of DNA, possibly due to intercalative mode of binding. The intrinsic binding constant K_b was determined by using Stern Volmer equation (1) [40].

$$[DNA]/[\varepsilon_a-\varepsilon_f]) = [DNA]/[\varepsilon_b-\varepsilon_f]+1/Kb[\varepsilon_b-\varepsilon_f] \quad (1)$$

From the binding constant K_b, the binding strength of the complexes with CT-DNA can be determined by monitoring the change in the absorbance in the intra ligand (IL) band with respect to the increasing concentration of DNA. K_b is obtained from the ratio of slope to the intercept in plots by DNA/(ε_a-ε_f) versus [DNA] (Fig. 3 Inset). From the binding constant values (Table 2), it is inferred that the complex **4** exhibited better binding than other complexes; it may due to the electron withdrawing phenyl substitution present in the ligand moiety of the complex. Based on the K_b value, we can arrange the complexes in the following order with respect to the electron delocalization, **4** > **3**>**1** > **2**.

The result obtained from the above experiments suggested that

Table 1
Crystallographic data of H_2L^1 and new Ru(II) thiosemicarbazone complexes.

	[H_2-DeaSal-tsc] (H_2L^1)	[RuCp(Dea-tsc)(PPh_3)](**1**)
CCDC No.	1500357	1500358
Empirical formula	$C_{12}H_{18}N_4OS$	$C_{35}H_{37}N_4OPRuS$
Formula weight	266.36	693.78
Temperature	293 K	293 K
Wavelength	1.54184 Å	0.71073 Å
Crystal system	Monoclinic	Triclinic
Space group	P $2_1/c$	P *-1*
a	11.4268(8) Å	11.0574 (2) Å
b	10.54035(17)Å	12.2568 (2) Å
c	18.7023(14)Å	12.2843 (3) Å
α	90.0°	92.6273 (19)°
β	141.678(16)°	95.153 (2)°
γ	90.0°	99.6015(17)°
Volume	1396.76(15)Å^3	1631.77(7) Å^3
Z	4	2
Calculated density	1.267 Mg/m^3	1.412 Mg/m^3
Absorption coefficient	2.021 mm^{-1}	0.627 mm^{-1}
F(000)	568	716
Crystal size	0.18 × 0.12 x 0.03	0.12 × 0.1 × 0.05 mm
Theta range for data collection	4.736 to 73.674	3.350–28.909°
Limiting indices	−14 = h<=10, −12 = k<=13, −20 = l<=22	−14 = h<=14, −16 = k<=16, −16 = l<=16
Reflections collected/unique	5184/2740 [R(int) = 0.0258]	32781/7581 [R(int) = 0.0326]
Completeness to theta	66.97° 100%	25.30° 99.78%
Absorption correction	Semi-empirical from equivalents	Semi-empirical from equivalents
Max. and min. transmission	1.00000 and 0.86588	1.00000 and 0.94103
Refinement method	Full-matrix least-squares on F^2	Full-matrix least-squares on F^2
Data/restraints/parameters	2740/0/166	7581/6/392
Goodness-of-fit on F^2	1.059	1.049
Final R indices [I > 2sigma(I)]	R1 = 0.0371, wR2 = 0.1051	R1 = 0.0426, wR2 = 0.0957
R indices (all data)	R1 = 0.0408, wR2 = 0.1106	R1 = 0.0561, wR2 = 0.1043
Largest diff. peak and hole	0.295 and −0.176 e.A^{-3}	0.788 and −0.754 e.A^{-3}

all the compounds can bind with CT-DNA. Further, the binding affinity of the complexes with the CT-DNA has been confirmed by Ethidium bromide (EB) displacement studies. Ethidium bromide competitive binding studies using new ruthenium(II) complexes **1**–**4** as quenchers may give the further information about the binding of these complexes to DNA. EB emits strong fluorescence in the presence of DNA, due to its strong intercalation with DNA base pairs. The quenching extent of fluorescence of EB bound to DNA is used to determine the extent of binding of metal complexes to DNA. When complexes **1**–**4** were added to DNA pretreated with EB, the DNA induced emission intensity at 602–606 nm was decreased (Fig. S27). This indicated that the complexes could replace EB from the DNA-EB system. Based on the classical Stern-Volmer equation (2) the quenching constant has been analyzed.

$$I_0/I = Ksv[Q] + 1 \quad (2)$$

The K_{sv} values have been obtained as a slope from the plot of I_0/I vs [Q] (Fig. S28) were evaluated for the complexes. Further, the apparent DNA binding constants (K_{app}) were calculated using equation (3):

$$K_{EB}[EB] = K_{app}[complex] \quad (3)$$

where [complex] is the value at 50% reduction in the fluorescence intensity of EB, K_{EB} (1.0×10^7 M^{-1}) is the DNA binding constant of EB, [EB] is the concentration of Ethidium Bromide (EB) (10 μM). K_{app} values are found (Table 2). From these experimental data, it is inferred that the complex **4** replaces the EB more effectively than other complexes. From this observation, it may conclude that all the complexes can bind to DNA through the intercalation mode [36].

3.1. DNA cleavage study

Agarose gel electrophoresis assay is a valuable method to examine various binding modes of small molecules to plasmid DNA. Natural derived plasmid DNA mainly contains closed-circle supercoiled form (Form I), nicked form (Form II) and linear form

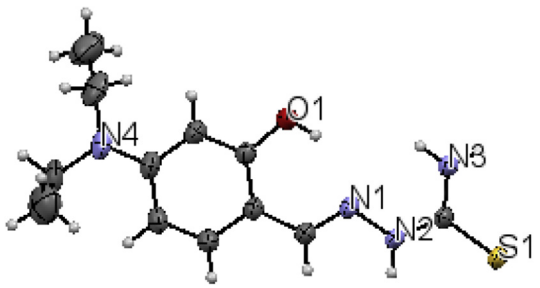

Fig. 1. ORTEP for [H_2-DeaSal-tsc] (H_2L^1).

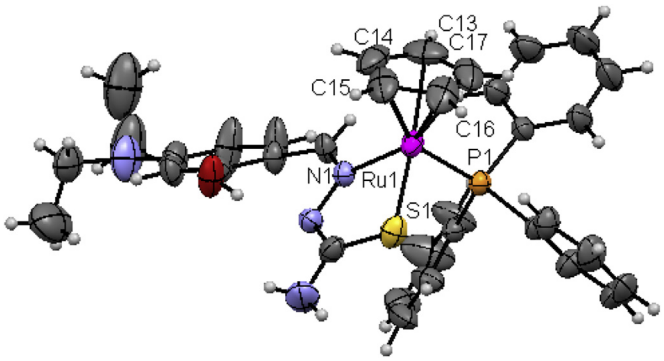

Fig. 2. ORTEP for [RuCp(DeaSal-tsc)(PPh3)](1).

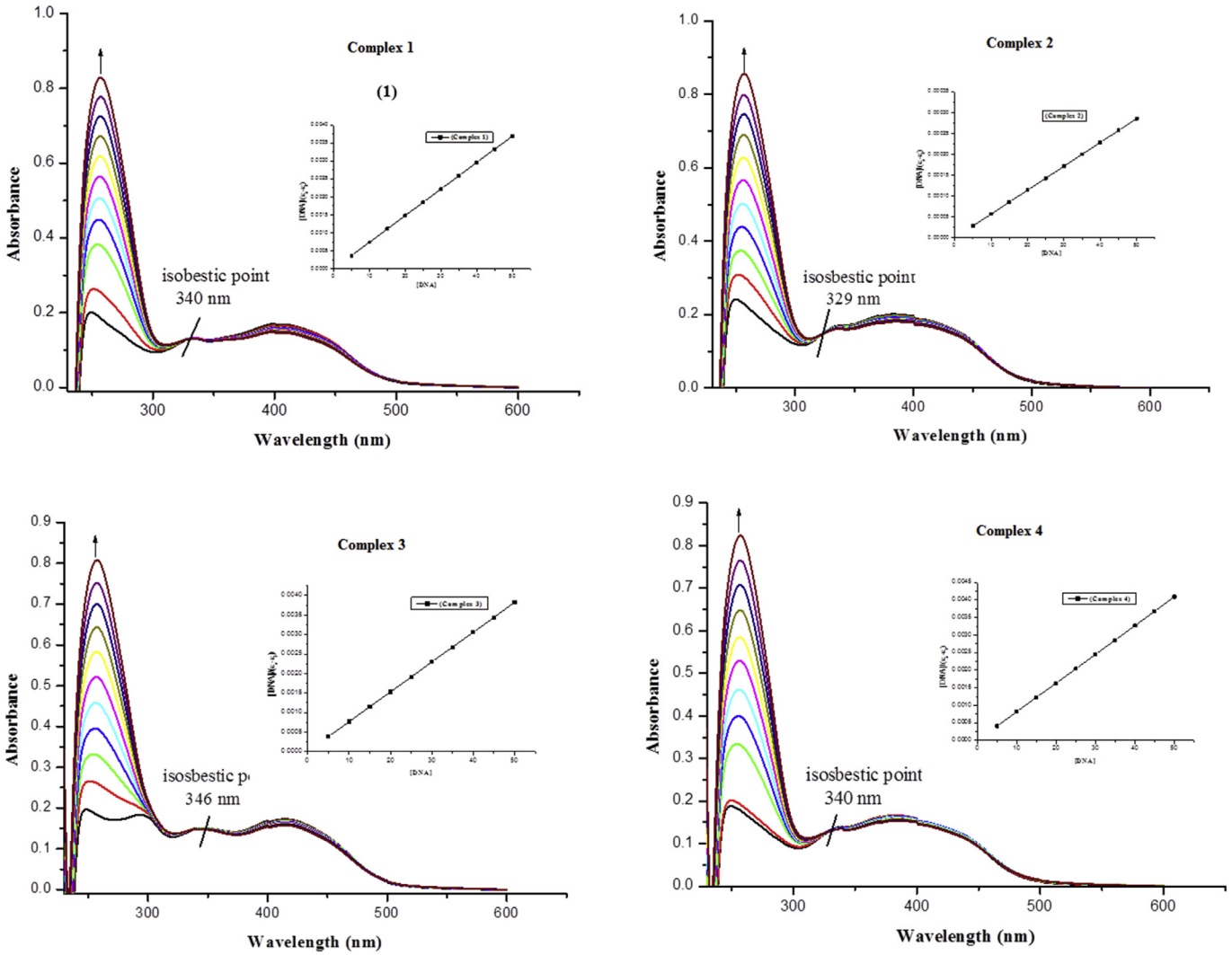

Fig. 3. Absorption titration spectra of complexes (10 μM) **1**–**4** with increasing concentrations (0–50 μM) of CT-DNA (trisHCl buffer, pH 7.2); the inset shows binding isotherms with CT-DNA.

(Form III). Intercalation of small molecules to plasmid DNA can cleave the supercoiled form of DNA, which decreases its mobility rate and can be distinctly visualized by agarose gel electrophoresis method. Morever, simple electrostatic contact of small molecules to DNA does not considerably influence the supercoiled form of plasmid DNA, thus does not change the mobility of supercoiled DNA. To identify the DNA cleavage ability of the free ligands and ruthenium(II) complexes, supercoiled (SC) pBR322 DNA was incubated with complexes and ligands in 5 mM Tris HCl/50 mM NaCl buffer at pH 7.2 for 2 h without reductant addition. Upon gel electrophoresis of the reaction mixture, DNA cleavage was observed (Fig. S29). The relatively fast migration is the supercoil form (Form I) and the slower migration is the open circular form (Form II), which was produced from supercoiled when scission occurred on its one strand [41]. The ligands and complexes at same concentration is able to perform cleavage of pBR322 plasmid DNA. The intensity of supercoiled SC (Form I) diminished and partly converted to nicked form NC (Form II) in ligands and in complexes (**2** and **3**) whereas in complexes (**1** and **4**), the intensity of supercoiled SC (Form I) increased and partly converted to nicked form NC (Form II). The intensity of the NC (Form II) band increases, whereas the production of linear form LC (Form III) of DNA diminished. It is obvious that the ligands and ruthenium(II) complexes have the ability to cleave the supercoiled plasmid DNA and this cleavage system does not require addition of any external agents.

Table 2
The $\mathbf{K_b}$(binding constant), $\mathbf{K_{sv}}$(Quenching constant) and $\mathbf{K_{app}}$(apparent with EB) values for the interactions of compounds with CT-DNA.

Complex	K_b/M^{-1}	K_{sv}/M^{-1}	K_{app}/M^{-1}
1	$2.21 \times 10^5 \pm 0.23$	$1.45 \times 10^4 \pm 0.01$	6.77×10^6
2	$0.40 \times 10^5 \pm 0.09$	$1.07 \times 10^4 \pm 0.07$	6.32×10^6
3	$3.82 \times 10^5 \pm 0.12$	$2.03 \times 10^4 \pm 0.04$	5.83×10^6
4	$4.08 \times 10^5 \pm 0.14$	$2.94 \times 10^4 \pm 0.03$	6.87×10^6

3.2. Absorption spectra of BSA

The general method to distinguish between static and dynamic quenching is by examining the absorption spectra of BSA (10 μM) in the presence of complexes. The absorption intensity of BSA was increased with the addition of the complexes (**1**–**4**) (Fig. S30). The increasing intensity in the absorbance spectra for BSA + complexes indicate the interaction of complexes with BSA. It is well known that dynamic quenching only disturbs the excited state of

fluorophore, thus shows no change the absorption spectrum. But, the formation of non-fluorescence ground-state complex induced the change in absorption spectrum of fluorophore. Thus, possible quenching mechanism of fluorophore-quencher (BSA) by the complexes was found as static quenching [42].

3.3. Fluorescence quenching studies of BSA

In order to infer more on the binding of the complexes with BSA (10 μM), fluorescence emission spectrum of BSA was studied upon addition of the complexes (**1**–**4**). BSA has three fluorophores, namely, tryptophan, tyrosine, and phenylalanine, but the intrinsic emission intensity of BSA is due to tryptophan alone, because phenylalanine has low quantum yield and the fluorescence of tyrosine is nearly quenched when it becomes ionized or near to an amino group, a carbonyl group, or a tryptophan residue [43]. Changes in the emission spectra of tryptophan are common in protein conformational transitions, substrate binding, subunit associations, or denaturation. Whereas, the interaction of BSA with our complexes (**1**–**4**) was studied at room temperature and the binding constants (**1**–**4**) were calculated. The fluorescence spectra were recorded in the range of 290–500 nm upon excitation at 280 nm. When the concentration of complexes increased (**1**–**4**), a gradual decrease in the fluorescence intensity was detected with a blue shift (Fig. S31). The blue shift was due to the binding of the complexes (**1**–**4**) with the active site in BSA [44]. The binding constant K_{SV} value was obtained from the plot of I_0/I_{corr} versus [Q] in Stern–Volmer equation (4) (Fig. S32 and Table S3).

$$I_0/I_{corr} = 1 + KSV[Q] \quad (4)$$

The observed linearity in the plots indicated the ability of complexes to quench the BSA emission intensity. From K_{SV} values, it is seen that the new complexes (**1**–**4**) showed strong protein-binding ability with greater hydrophobicity.

3.4. Binding constants and the number of binding sites

For the static quenching interaction, if it is considered that there are similar and independent binding sites in the biomolecule, the binding constant (K_b) and the number of binding sites (n) can be determined according to the Scatchard equation (5) [45]. $\log [(I_0-I)/I] = \log K_b + n \log [Q]$ (5) The values of n at room temperature are approximately equal to 1, which indicates that the complexes bind with BSA in one site only (Fig. S33 and Table S3).

3.5. Synchronous fluorescence spectroscopic studies of BSA

Synchronous fluorescence spectral study was used to obtain information about the molecular environment in the vicinity of the fluorophore moieties of BSA [46]. Synchronous fluorescence spectra showed tyrosine residues of BSA only at the wavelength interval Δλ of 15 nm whereas tryptophan residues of BSA at Δλ of 60 nm. While increase the concentration of complexes (0–50 μM) added to BSA (10 μM), a decrease in the fluorescence intensity with a blue shift in the tryptophan emission maximum is observed for all the complexes (Fig. S34). In contrast, the emission intensity of tyrosine residue increases without any change in the wavelength of emission. These observations indicate that the test compounds did not affect the microenvironment of tyrosine residues during the binding process significantly but the tryptophan microenvironment to a larger extent.

3.6. In vitro antioxidant study

Since the experiments conducted so far revealed that the Ru(II) complexes exhibit good DNA and protein binding affinity, it is considered worthwhile to study the antioxidant activity of these complexes (Fig. 4). Antioxidants that exhibit radical scavenging activity are receiving increased attention since they present interesting anticancer, anti-aging and anti-inflammatory activities [47]. The radical scavenging activities of our compounds along with standards, ascorbic acid in a cell free system, have been examined with reference to 2,2-diphenyl-1-picrylhydrazyl (DPPH). and their corresponding IC_{50} values have been tabulated in Table S4. The power of the complexes ability to scavenge DPPH radicals was found to be higher than that of the standard antioxidant (ascorbic acid), Thus the scavenging ability of the Ru(II) complexes was most appreciable for DPPH radicals when compared to the standards. The IC_{50} values indicated that the activities of the complexes are in the order of **4** > **3**>**1** > **2**.

3.7. Toxicity testing assay

Dose dependent studies on a beneficial and adverse effect of the synthetic antioxidant such as BHA on animal models were investigated [48]. The preliminary assay was conducted at 20 °C in 48 well plates according to the previous method [49]. The dose dependent toxicity at 100 μM and 200 μM in all the complexes were found after 24 h treatment. The Fig. 5 showed the percentage survival of adulthood worms at selected molarities. The results showed that the increase in the concentration of the complexes, the toxicity increases. The concentration 100 and 200 μM showed toxic to the worms and hence the remaining concentrations *viz*., 10, 30 and 50 μM were taken for further studies.

3.8. Oxidative stress resistance assay

In general oxidative stress resistance is proportional to the superoxide dismutase and catalase activity in *C. elegans* [50]. The oxidative stress resistance on wild type (N2) strain were presented in the (Fig. 6). Two days old adult N2 worms were pre-treated with 10, 30 and 50 μM of four complexes and transferred into 240 μM Juglone plates for 5 h. Worms were considered as dead if they are not responding to gentle touch. Juglone is a redox cycling pro-oxidant that generate O_2^-, H_2O_2 and OH leads to death [51]. The survival percentage against the oxidative stress was observed 34.54, 50.76 and 62.46 % in complex **1**; 33.28, 45.59 and 53.19 % in complex **2**; 33.51, 48.54 and 59.26 % in complex **3**; 38.69, 55.78 and 65.05 % in complex **4** at 10, 30 and 50 μM concentrations respectively. The complex **4** holds a higher scavenging activity and attenuate oxidative damage in *C. elegans*. The results of oxidative

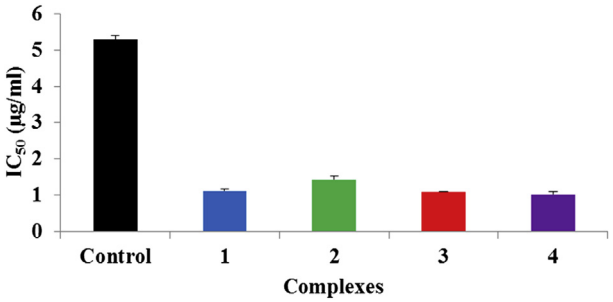

Fig. 4. *In vitro* free radical scavenging activity of complexes (**1**–**4**) with control ascorbic acid. DPPH Scavenging activity in the sample is denoted by IC_{50} (μg/ml) value. Three independent experiments were carried and bar represents the mean ± S.E.M.

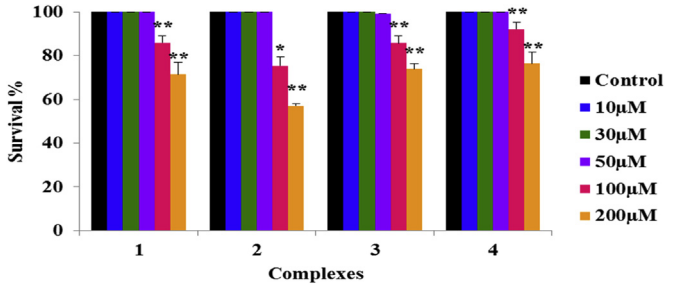

Fig. 5. The toxicity assay was conducted in two day adult worms at 20 °C for 24 h. The survival rate was significantly reduced proportional to increasing concentrations in all four derivatives. An approximately ≥30 worm per group was taken and three independent biological experiment were conducted. The means of control and treatment were compare with one way analysis of variance (ANOVA) using statistical software SPSS v. 16.0. The error bar represents the mean ± S.E.M. $^{**}p = 0.0001$ and $^{*}p = 0.001$.

stress resistance clearly shown that the complexes having a great intracellular ROS scavenging activity. The antioxidants like 4-hydroxybenzoic acid and curcumin are intracellular free radical scavengers that increase *mev-1* mutant lifespan and resistance to oxidative stress in wild type (N2) worms confirm that oxidative stress resistance in wild type is correlated with *mev-1* mutant lifespan extension in *C. elegans* [52]. However, one form of catechin, epigallocatechingallate ([(2R,3R)-5,7-dihydroxy-2-(3,4,5-trihydroxyphenyl) chroman-3-yl] 3,4,5-trihydroxybenzoate) increases oxidative stress resistance and decreases Aβ peptide aggregation in muscles by either direct or indirect activation of DAF-16 nuclear localization [53].

3.9. Lifespan assay

The *in vivo* antioxidant activities of complexes (**1**–**4**) were investigated with the mutant strain *mev-1* (Fig. 7). Mutation in succinate dehydrogenase *cytochrome b* encoding gene *mev*-1(*kn1*) in *C. elegans* cause overproduction of superoxide anions which leads to short lifespan [54,55]. Previous studies with the antioxidant 4-hydroxybenzoic acid extend the lifespan of *mev-1* mutants worms. This indicates the antioxidant potential of the compound that could reduce the oxidative damage which could lead to increase in lifespan of *C. elegans* [52]. In the present study we observed mean lifespan of *C. elegans* increased overall in four derivatives. The Table S5 showed the mean lifespan and percentage increase in *mev*-1 mutant lifespan at 20 °C. In the present

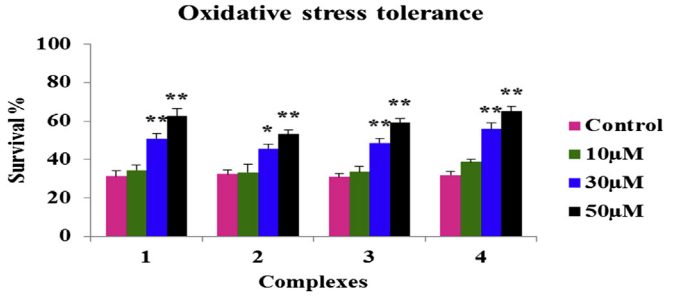

Fig. 6. Synchronized L1 larvae (as described in lifespan assay) of N2 worms were transferred to NGM plates previously supplemented with respective dosage of all complexes at 20 °C. Subsequently day 2 adult N2 worms were transferred to treatment plates contains acute lethal concentration of juglone (5-Hydroxy-1,4-napthoquinone) an intracellular ROS generator at 240 µM concentration. Survival was calculated after 5 h of exposure. The means of control and treatment were compare with one way analysis of variance (ANOVA) using statistical software SPSS v. 16.0. The error bar represents them mean ± S.E.M. $^{**}p = 0.0001$ and $^{*}p = 0.001$.

experiment the complex **4** has significant increase in longevity of *C. elegans* than others. At 50 µM the complex **4** extent the mean lifespan of *mev-1*mutant into 22.4%, ($p < 0.0001^{***}$) and this final concentration was used for analyse the *sod-3* expression and DAF-16 nuclear localization using GFP tagged strains.

The *mev-1* mutant worms were treated with all four complexes with different concentrations from L4 (young adult) stage until the completion of lifespan. The complex **4** significantly increased the mean lifespan on a dose dependent manner. As the highest antioxidant and longevity was found for complex **4**, we further used complex **4** alone to confirm daf-16 mediated activity by applying on strain TJ356 and CF1553.

3.10. DAF-16 nuclear localization and SOD-3 expression analysis

The *daf*-16 is a key activator for resistance and extension of lifespan under stress condition which activate pro-longevity genes and it is negatively regulated by Insulin/Insulin like growth factor −1(IIS) [56–58]. Activated DAF-16 transcription factor into to nucleus and stimulates stress resistant genes, which confer resistance to oxidative damage. In this study we observed that DAF-16 nuclear translocation is induced by **4** at 50 µM suggesting that DAF-16/FOXO-dependent longevity is mediated by expression of multiple target genes [57]. The (Fig. 8) showing the nuclear localization of DAF-16::GFP in the transgenic worm TJ356. We further analyzed the DAF-16 target gene *sod-3* expression using SOD-3::GFP tagged transgenic strain CF1553. Superoxide dismutase and heat shock protein are direct target genes of DAF-16 transcription factor. The (Fig. 9) showing the expression of *sod-3* treated with complex **4** at 50 µM and 0.2% DMSO for 72 h to reach second day adult after immediately transferred into new plates exposed with 40 µM juglone for 24 h and visualized under at excitation emission of 450–520 nm in fluorescent microscope. Our result confirmed that the expression of SOD-3 is higher than control suggesting that the complex **4** partially or indirectly activate DAF-16 and extend the lifespan and resistance to oxidative stress through the DAF-16/FOXO dependent pathway in *C. elegans*. Present study suggest that the test complex **4** might extend the mean lifespan as previously reported with antioxidant kaempferol [59–62], (Fig. 10). In this study we conclude that complex **4** have the potential anti-aging activity in two parallel ways by stimulate DAF-16 nuclear movement and free radical scavenging activity *in vivo*.

3.11. Amyloid − β induced paralysis assay

Paralysis assay was performed with transgenic strain CL4176 a temperature inducible strain expressing amyloid beta (Aβ) in its muscle cells. While increasing the temperature from 16 °C to 25 °C induces the human Aβ expression in body wall muscle cells resulting paralysis phenotype [63]. To examine whether the complexes has protective effects on Alzheimer's disease (AD), the synchronized L1 larvae of CL4176 were cultured on NGM plates previously spotted with 50 µM of complexes (**1**–**4**) and maintained 50 h at 16 °C. After that the temperature were raised to 25 °C to induce the Aβ toxic peptide for muscle paralysis (Fig. 11). Paralysis was noticed in the worms fed with complexes (**1**–**4**) at 50 µM concentration compared to control group worms ($p; < 0.0001$). The lowest paralysis was found in the complex **4** than rest of the complexes. Also the result suggested that all the complexes had protective role against Aβ toxicity in CL4176 transgenic *C. elegans*.

Oxidative stress plays a vital role in the pathogenesis of Alzheimer's disease which significantly affects the nervous system and their functions. The inhibitory effects of Aβ *toxic peptide* accumulation by anti-oxidants have been demonstrated through both

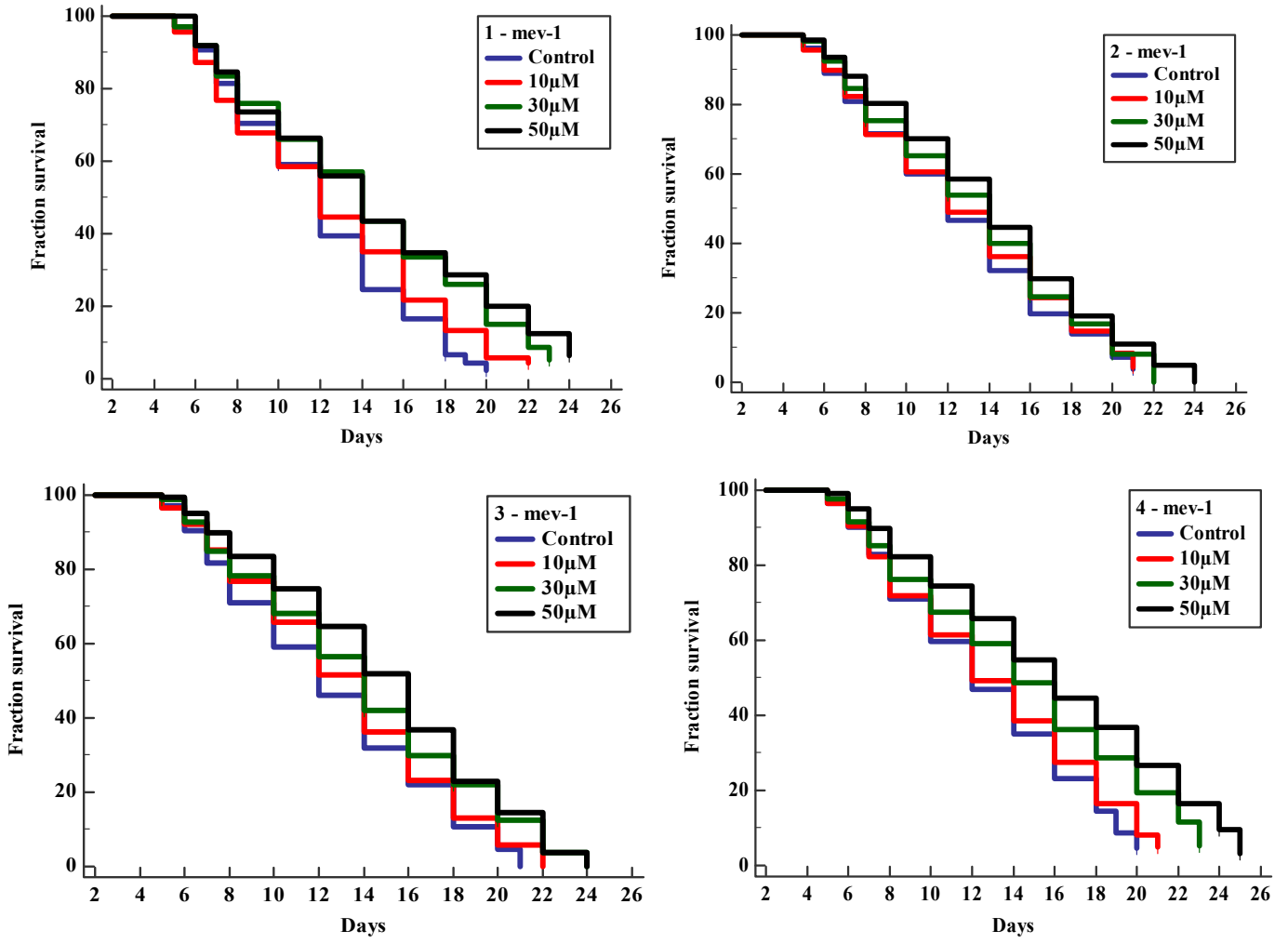

Fig. 7. Effect of complexes on the *C. elegans mev*-1 (*kn1*) mutants which overproduce ROS. The **complex 1** at 50 µM significantly extend mean lifespan 14.47 ± 0.45 days than control (12.14 ± 0.33, $p < 0.0001^{***}$) (1). **Complex 2** at 50 µM significantly extent mean lifespan 14.28 ± 0.34 days than control (12.61 ± 0.34, $p < 0.0001^{***}$). (2). **Complex 3** at 50 µM significantly extent mean lifespan 14.84 ± 0.32 days than control (12.67 ± 0.35, $p < 0.0010^{**}$). (3). **Complex 4** at 50 µM significantly extend the mean lifespan 15.49 ± 0.42days than control (12.64 ± 0.33, $p < 0.0001^{***}$) (4). Three independent experiment were conducted and the statistical significance of the survival curve were processed using log rank test using the Kaplan–Meir survival analysis in Med Calc software version 14.8.1.0.

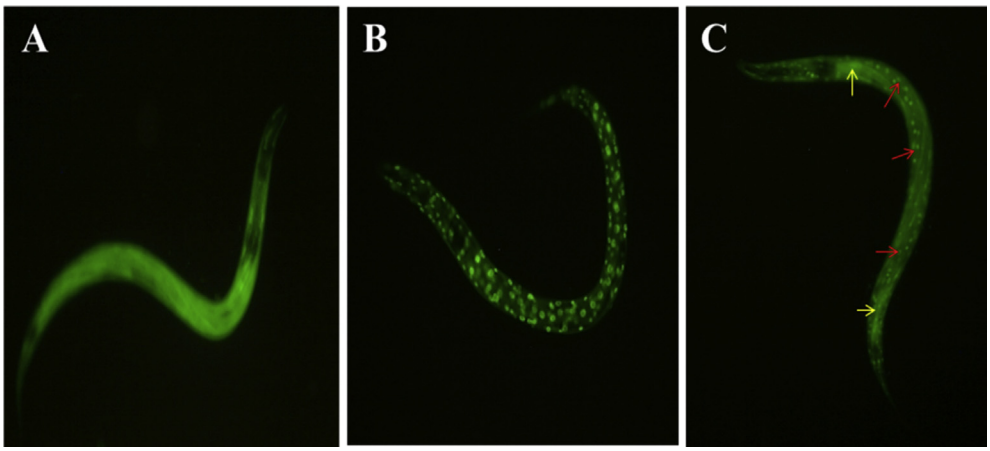

Fig. 8. Effects of thermal stress and complex **4** on nuclear translocation of DAF-16 in TJ356 transgenic worms. **A**. Negative control (without any treatment); **B**. Thermal stress at 37 °C for 15 min (positive control); C. Partial nuclear translocation of DAF-16 induced by 50 µM complex **4**. At least 20 worms were performed. RED colour arrow indicates the nuclear localization and YELLOW colour arrow indicates the cytoplasmic localization. (For interpretation of the references to colour in this figure legend, the reader is referred to the web version of this article.)

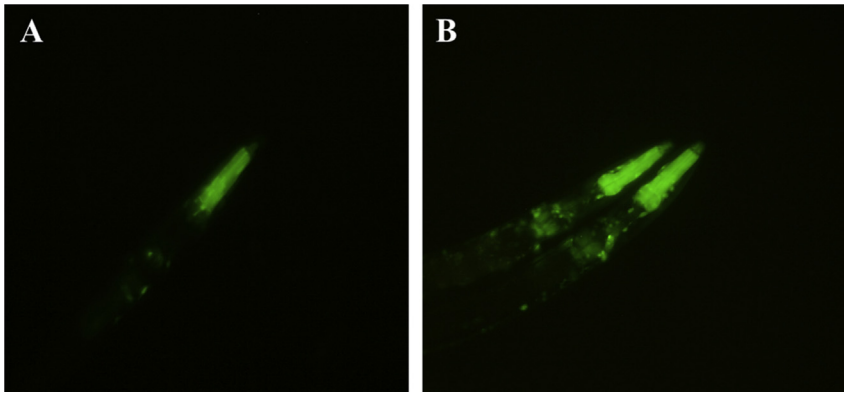

Fig. 9. Complex **4** up-regulates the expression of stress response gene sod-3 in CF1553 (SOD-3::GFP). **A**. Control worms (without any treatment); **B**. Worms treated with 50 μM of complex **4**.

in vitro and *in vivo* models [64]. Free radical scavengers have healing effects with respect to chronic and degenerative diseases. Furthermore, it is believed that the anti-amyloid accumulation effects of complexes are considerably associated to their anti-oxidative abilities.

4. Conclusion

The four new complexes, (**1**–**4**) were synthesized and characterized by elemental analyses, various spectroscopic techniques (NMR, UV–Vis, IR) and X-ray crystallography. In all the complexes, the ligand coordinated in a bidentate monobasic fashion by forming a stable NS five-member ring in 65–69% yield. Comparative biological studies such as DNA, protein binding have been carried out for new ruthenium(II) complexes (**1**–**4**). From the DNA binding studies, it is inferred that all the complexes exhibited electrostatic binding modes. The complex **4** showed better binding which is supported by further biological studies. The protein binding studies have been monitored by quenching of tryptophan and tyrosine residues in the presence of compounds by taking bovine serum albumin (BSA) as a model protein and the mechanism of quenching was found as static. The biological activity concludes that the complexes **1**–**4** increase the protection from oxidative damage and up regulating antioxidant gene *sod*-3 in *C. elegans*. Our further study in strain *mev-1*(*kn1*) and the worm expressing human amyloid protein $A\beta_{3\text{-}42}$ (CL4176) confirm that the complex **4** increase the maximum lifespan through direct scavenging or up regulating antioxidant responsible genes and inhibit Aβ deposits respectively.

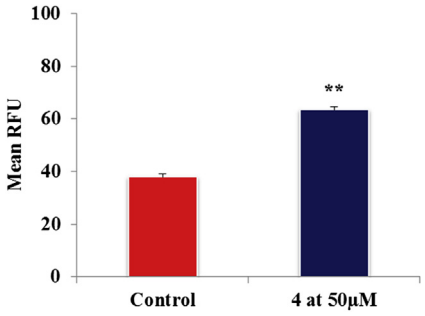

Fig. 10. SOD-3 expression by treatment with complex **4** at 50 μM and control 40 μM juglone on CF1553. Young adult N2 worms treated two days with complex **4** then transferred into 40 μM juglone for 1 day. The nematode were then transferred into 30 μM sodium azide agar pad for anesthetized. The florescence intensity of GFP was quantified in the worm's pharynx from at least 30 worms. Error bar represent mean ± S.E.M, **p; < 0.001. The florescence intensity were quantified by Image J software.

Based on the results we confirmed, complexes **4** have linked with DAF-16/FOXO mediated lifespan extension and antioxidant properties of complexes.

5. Experimental section

All the reagents used were analar grade, were purified and dried according to the standard procedure [65]. The ligands ($\mathbf{H_2L^{1-4}}$) [66] and the ruthenium complex $[RuCl(PPh_3)_2(\eta^5\text{-}C_5H_5)]$ [67] were synthesized according to the standard literature procedures.

5.1. Measurements

Melting points were measured in a Lab India apparatus. Infrared spectra were measured as KBr pellets on a Jasco FT-IR 400-4100 cm^{-1} range. Elemental analyses of carbon, hydrogen, nitrogen, and sulphur were determined using Vario EL III CHNS at the Department of chemistry, Bharathiar University, Coimbatore, India. Electronic absorption spectra of the compounds were recorded using JASCO 600 spectrophotometer and emission measurements were carried out by using a JASCO FP-6600 spectrofluorometer.

^1H, ^{13}C and ^{31}P NMR spectra were recorded in $CDCl_3$ and DMSO at room temperature with a Bruker 400 MHz instrument, chemical shift relative to tetramethylsilane. The chemical shifts are expressed in parts per million (ppm). CT-DNA, pBR322 plasmid DNA, BSA and ethidium bromide (EB) were obtained from Hi media. Single crystal data collections and corrections for the ligand (H_2L^1) and new Ru(II) complexes 1 were done at 293 K with CCD Kappa Diffractometer using graphite mono chromated Mo Ka (k = 0.71073 A) radiation [68]. The structural solution were done by using SHELXS-97 [69] and refined by full matrix least square on *F2* using SHELXL-2014 [70].

5.2. Synthesis of new ruthenium(II) complexes

5.2.1. Synthesis of [RuCp(DeaSal-tsc)(PPh$_3$)] (**1**)

To a metanolic solution (10 cm^3) of $[RuCl(PPh_3)_2(\eta^5\text{-}C_5H_5)]$ (0.05 g, 0.0688 mmol), 4(*N,N′*)-diethylaminosalicylaldehydethiosemicarbazone [H_2-DeaSal-tsc] (0.018 g, 0.0688 mmol) in methanol (10 cm^3) was added. The reaction mixture was then refluxed for 5 h. The reddish orange suspension gradually turned orange colour. The solvent was removed under reduced pressure. The orange solid was washed with petroleum ether (60-80 °C) 2–3 times to remove traces of triphenylphosphine. The complex was dissolved in CH_2Cl_2/*n*-hexane and kept for crystallisation. On slow evaporation orange crystals were obtained. Yield: 67%. Mp 132 °C. Anal. calcd for $C_{35}H_{37}N_4OPRuS$: C, 60.59; H, 5.38; N, 8.08; S, 4.62. Found: C, 60.55;

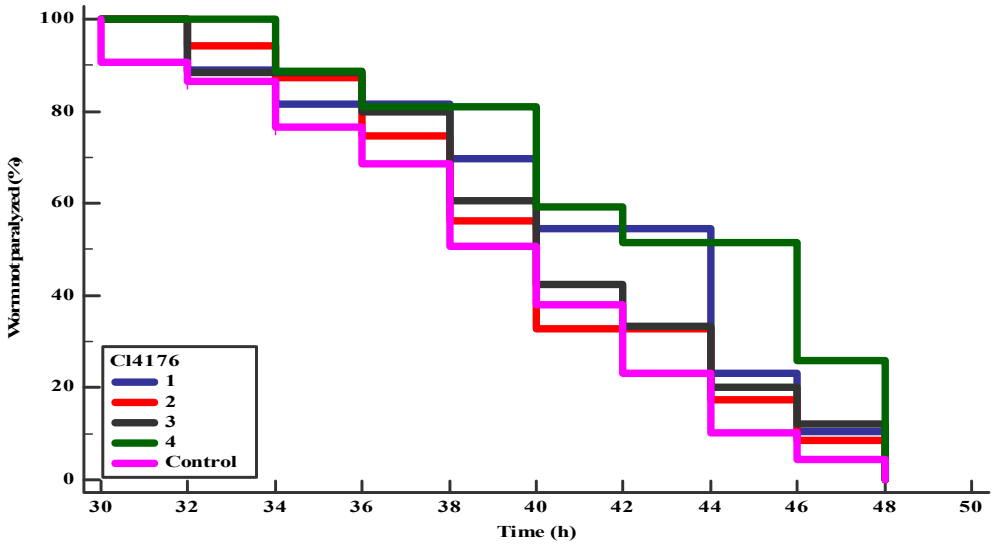

Fig. 11. Effects of complexes (1–4) on *C. elegans* transgenic strain CL4176 expressing a temperature inducible expression of amyloid beta (Aβ) in its body wall muscles. Synchronized larvae of strain CL4176 were transferred to NGM with *E. coli* OP50 and 50 μM concentration of each complex for 50 h at 16 °C. After that the temperature was up-shift to 25 °C to induce the expression of muscle specific Aβ transgene expression. The paralysis was scored at every 2 h intervals until the last worm become paralyzed. Data are expressed as percentage of non-paralyzed worms from three independent biological replicates with 100 worms in each set of experiments. Statistical significance of the dissimilarities between the treated and untreated control was validated by log-rank test using the Kaplan-Meier survival analysis using Med Calc v.14. Differences at the $p < 0.05$ level were considered as significantly different.

H, 5.37; N, 8.00; S, 4.59%. FT-IR (cm^{-1}) in KBr: 3432(υ_{O-H}), 1577 ($\upsilon_{C=N}$), 1351 (υ_{C-O}), 747 (υ_{C-S}), 1421, 1023, 695 cm^{-1} (for PPh_3); UV-Vis (CH_2Cl_2), λ_{max}: 233 (65,890) nm ($dm^3\ mol^{-1}cm^{-1}$) (intra-ligand transition); 351 nm (21,353) ($dm^3\ mol^{-1}cm^{-1}$) (LMCT); ^{1}H NMR ($CDCl_3$, ppm): 11.61 (s, H, −OH), 4.33 (s, 5H, C_5H_5), mixed with aromatic region (s, 1H, - CH=N), 9.48 (s, 2H, terminal $-NH_2$), 3.08–3.12 (q, 2H, $J = 7$ Hz, $-CH_2N$), 1.13–1.16 (t, 3H, $J = 7$ Hz,-CH_3), 7.29–7.69 (m, aromatic protons); ^{13}C NMR ($CDCl_3$, ppm): 165.21(C–S), 159.94 (C=N),79.91 (Cp),158.20 (C–O), 140.77 (C–N), 127.82–134.40 (aromatic C);^{31}P NMR ($CDCl_3$ ppm): 29.28 (s).

A similar method was followed to synthesize other complexes.

*5.2.2. Synthesis of [RuCp(DeaSal-mtsc)(PPh$_3$)] (**2**)*

Complex **2** was prepared by the procedure as described for (**1**) with 4(*N,N′*)-diethylaminosalicylaldehyde-4(*N*)-methylthiosemicarbazone [H_2-DeaSal-mtsc] (0.019 g, 0.0688 mmol). Orange red solid formed was filtered, washed with petroleum ether (60–80 °C) and recrystallized from dichloromethane and hexane. Yield: 64%. Mp: 118 °C. Anal. Calcd for $C_{36}H_{39}N_4OPRuS$: C, 61.09; H, 5.55; N, 7.92; S, 4.53. Found: C, 61.12; H, 5.50; N, 7.89; S, 4.50%. FT-IR (cm^{-1}) in KBr: 3432(υ_{O-H}), 1562 ($\upsilon_{C=N}$), 1273 (υ_{C-O}), 749 (υ_{C-S}), 1422, 1022, 695 cm^{-1} (for PPh_3); UV-Vis (CH_2Cl_2), λ_{max}: 233 (62,223) nm ($dm^3\ mol^{-1}cm^{-1}$) (intra-ligand transition); 383 (28,668) nm ($dm^3\ mol^{-1}cm^{-1}$) (LMCT); ^{1}H NMR ($CDCl_3$, ppm): 11.62 (s, 1H -OH), 4.34 (s, 5H, C_5H_5), 7.88 (s, 1H, - CH=N), 9.60 (s, 1H, terminal NH), 3.09–3.14 (q, 2H,J = 7.5 Hz,-CH_2N-), 1.39–1.42 (t, 3H,J = 7.5 Hz,-CH_3), 2.78–2.79 (d, 3H,$J = 5$ Hz, terminal CH_3), 6.02–7.88 (m, aromatic protons;^{13}C NMR ($CDCl_3$, ppm): 169.40(C–S), 162.16 (C=N), 80.19 (Cp), 145.19 (C–O), 139.56 (C–N), 128.28–133.31 (aromatic PPh_3); ^{31}P NMR ($CDCl_3$ ppm): 29.44 (s).

*5.2.3. Synthesis of [RuCp(DeaSal-etsc)(PPh$_3$)] (**3**)*

Complex **3** was prepared by the procedure as described for (**1**) with 4(*N,N′*)-diethylamino salicylaldehyde-4(*N*)-ethylthiosemicarbazone [H_2-DeaSal-etsc] (0.019 g, 0.0688 mmol). Orange red solid formed was filtered, washed with petroleum ether (60–80 °C) and recrystallized from dichloromethane and hexane. Yield: 66%. Mp. 151 °C. Anal. calcd for $C_{37}H_{41}N_4OPRuS$: C, 61.56; H, 5.72; N, 7.76; S, 4.44. Found: C, 61.51; H, 5.68; N, 7.74; S, 4.41%. FT-IR (cm^{-1}) in KBr: 3404(υ_{O-H}), 1563 ($\upsilon_{C=N}$), 1267 (υ_{C-O}), 743 (υ_{C-S}), 1417, 1026, 694 cm^{-1} (for PPh_3); UV-Vis (CH_2Cl_2), λ_{max}: 234 nm (66,639) ($dm^3\ mol^{-1}cm^{-1}$) (intra-ligand transition); 335 (27,780), 390 (37,662) ($dm^3\ mol^{-1}cm^{-1}$) nm (LMCT); ^{1}H NMR ($CDCl_3$, ppm): 11.62 (s, 1H, −OH), 4.34 (s, 5H, C_5H_5), 7.00–7.02 (d, 1H, $J = 9$ Hz,- CH=N), 9.71 (s, 1H, NHC_2H_5), 3.09–3.13 (q, 2HJ = 7 Hz,-NCH_2–), 1.39–1.42 (t, 3HJ = 7.5 Hz, $-CH_3$), 1.04–1.07 (t, 3HJ = 7 Hz, terminal CH_3), 3.71–3.77 (p, 2H, $J = 7$ Hz, terminal CH_2) 6.05–7.89 (m, aromatic protons);^{13}C NMR ($CDCl_3$, ppm): 167.41(C–S), 162.67 (C=N),83.35 (Cp),136.31 (C–O), 142.84 (C–N), 119.60–133.95 (aromatic PPh_3); ^{31}P NMR ($CDCl_3$ ppm): 29.36 (s).

*5.2.4. Synthesis of [RuCp(DeaSal-ptsc)(PPh$_3$)] (**4**)*

Complex **4** was prepared by the procedure as described for (1) with 4(*N,N′*)-diethylamino salicylaldehyde-4(*N*)-phenylthiosemicarbazone [H_2-DeaSal-ptsc] (0.020 g, 0.0688 mmol). Orange solid formed was filtered, washed with petroleum ether (60–80 °C) and recrystallized from dichloromethane and hexane. Yield: 68%. Mp. 125 °C. Anal. calcd for $C_{41}H_{41}N_4OPRuS$: C, 63.96; H, 5.37; N, 7.28; S, 4.16. Found: C, 64.01; H, 5.35; N, 7.22; S, 4.13%. FT-IR (cm^{-1}) in KBr: 3426(υ_{O-H}), 1501 ($\upsilon_{C=N}$), 1228 (υ_{C-O}), 745 (υ_{C-S}), 1425, 1085, 691 cm^{-1} (for PPh_3); UV-Vis (CH_2Cl_2), λ_{max}: 234, 281 nm ($dm^3\ mol^{-1}cm^{-1}$) (intra-ligand transition); 403 nm ($dm^3\ mol^{-1}cm^{-1}$) (MLCT); ^{1}H NMR ($CDCl_3$, ppm): 11.62 (s, 1H, −OH), 4.30 (s, 5H, C_5H_5), 8.00 (1H, s, - CH=N), 9.48 (s, 1H, −NHPh), 3.09–3.13 (q, 2H, $J = 7$ Hz, $-CH_2-$), 1.39–1.42 (t, 3HJ = 7.5 Hz, $-CH_3$), 6.19–7.61 (m, aromatic protons);^{13}C NMR ($CDCl_3$, ppm): 165.21(C–S), 159.94 (C=N), 79.91 (Cp),144.87 (C–O), 159.02 (C–N), 127.82–134.40 (aromatic PPh_3);^{31}P NMR ($CDCl_3$ ppm): 29.40 (s).

6. Biological study

6.1. DNA binding study

The DNA binding experiments of the compounds with CT DNA were carried out according to the standard literature procedure [40].

6.2. DNA cleavage study

The cleavage of DNA was checked using agarose gel electrophoresis. Supercoiled pBR322 DNA (100 ng) in 5% DMSO and 95% Tris buffer (5 mM, pH 7.2) with 50 mM NaCl was incubated at 37 °C in the absence and presence of compounds (50 μM). The DNA, compound, and sufficient buffer were premixed in a vial, and the reaction was allowed to proceed for 2 h at 37 °C before the addition of ethylene glycol and loading onto an agarose gel. Agarose gel electrophoresis of plasmid DNA was performed at 50 V in 1% slab gels containing 0.5 μg mL^{-1}ethidium bromide in Tris buffer. DNA was visualized by photographing the fluorescence of intercalated ethidium bromide under a UV illuminator. The cleavage efficiency was measured by determining the ability of the compounds to convert the supercoiled (SC) DNA to the nicked circular (NC) form and linear circular (LC) form. After that the gel was documented on a Digital Gel Documentation system unit (Syngene, USA).

6.3. Competitive binding with ethidium bromide

To observe the mode of attachment of CT DNA to the complexes fluorescence quenching experiments of EB-DNA were carried out by adding 0–50 μM compounds containing 10 μM EB, 10 μM DNA and tris-buffer (pH = 7.2). Before measurements, the system was shooked and incubated at room temperature for approximately 5 min. The emission was recorded at 530–750 nm. The quenching extents of complexes were calculated qualitatively by employing Stern–Volmer equation (5).

$$I_0/I = K_{sv}[Q] + 1 \quad (5)$$

where I_0 is the emission intensity in the absence of compound, I is the emission intensity in the presence of compound, K_{sv} is the quenching constant, and [Q] is the concentration of the compound. The K_{sv} values have been obtained as a slope from the plot of I_0/Ivs [Q].

6.4. Protein binding study

The protein binding study of complexes with BSA was performed according to the standard literature method [40].

6.5. Antioxidant study

The 2,2-diphenyl-1-picrylhydrazyl (DPPH) radical scavenging activity of the compounds was measured according to the Braca method [71]. Different concentration of complexes (0.5–2.5 μg/ml) were prepared and subjected to antioxidant tests. Briefly 0.1 ml of complexes from final concentration of the solution was added with 0.9 ml distilled water and 3 ml of 0.1 mM DPPH in methanol to made for 4 ml, followed by incubation at 27 °C, for 30 min following the absorbance were determined at 517 nm. The percentage inhibition activity was calculated according to the formula $[(A_0–A_1)/A_0] \times 100$, where A_0 is the absorbance of the control, and A_1 is the absorbance of the extract/standard. Inhibition activity and IC_{50} values were obtained. Ascorbic acid was used for positive control and methanol used as negative control. The mean values were obtained from three independent experiments.

6.6. Strains and maintenance

Nematode culture and maintenance was performed according to the previously described method [72]. Strains used for this study *viz.*, **Bristol N2**, wild type; **TK22**,*mev-1* (*kn1*); **CF1553**, muIs84 (*sod*-3p::GFP + rol-6); **TJ356**, zIs356 (*daf-16*::GFP + rol-6); **CL4176**, *smg*-*1*(cc546) I; dvls27 and *E. coli* **OP50** were obtained from *Caenorhabditis* Genetic Centre (CGC, University of Minnesota, Minneapolis, MN, USA). For all the experiments, age synchronized populations were obtained by treating the gravid adult animals with 5% NaOCl and 5 N NaOH.

6.7. Toxicity testing assay

Toxicity assay was performed to eliminate the toxic concentration of worms as described previously [51]. In brief, age sorted late L4 stage wild type worms (n = 30) were treated with complex **1**–**4** at five test concentrations (10, 30, 50, 100 and 200 μM) in K-medium previously seeded with *E. coli* OP50 (6 μg/ml) as a sole food source and maintained at 20 °C for 24 h. Afterwards, the worms observed for inactivity under stereo zoom microscope. Both 100 and 200 μM test concentrations were found to be toxic to worms, hence we excluded these concentrations for further experiments.

6.8. Oxidative stress tolerance

For oxidative stress tolerance assay, age synchronized N2 worms were grown from L1 to L4 stage on the nematode growth medium (NGM) supplemented with complex **1**–**4** or 0.3% DMSO as a solvent control. At late L4 stage (6th day adulthood), the worms were subsequently transferred to new NGM plates consists of 240 μM juglone, an intracellular ROS generator for 5 h. After the exposure period the survival rate of the worms were confirmed by pharyngeal pumping and gentle physical touch with loop. Three independent biological replicates were performed.

6.9. Lifespan assay

Lifespan assay was conducted at 20 °C with mitochondrial mutant strain TK-22 (*mev-1*) which is sensitive to oxidative stress due to the over production of ROS. Synchronized L1 stage worms were placed on the NGM plates seeded with *E. coli* OP50 contains three concentrations (10, 30 and 50 μM) of complexes 1–4 and 0.3% DMSO as control. 50 μM of 5-Fluoro-2′deoxyuridine (FUdR) was also added to NGM plates to prevent the progeny development until the reproduction becomes ceased. Then the worms were counted and transferred to new treatment plates on every other day until the last worm become marked as dead or censored. The mean lifespan was calculated as the average number of days the worms survived in each test concentrations. The statistical significance of the survival curve were processed using Kaplan–Meir survival analysis (log rank test) in Med Calc software version 14.8.

6.10. DAF-16 nuclear localization and SOD-3 expression

The nuclear localization of DAF-16/FoxO transcription factor and SOD-3 expression was visualized using transgenic reporter strain TJ356 and CF1553 which express DAF-16::GFP and SOD-3::GFP fusion protein that is an ideal tool to assess the activity of complexes respectively. Late L4 stage worms of both strains were cultured on NGM plates contains complex **4** at 50 μM or 0.3% DMSO as a negative control for 4 days. A short thermal stress at 37 °C for 15 min and 40 μM juglone served as a positive control for TJ356 and CF1553 worms correspondingly. After that the worms were anesthetized with 30 mM sodium azide and mounted on agar pads. The DAF-16 nuclear localization and SOD-3 expression was visualized under Olympus fluorescence microscope adopted with Nikon camera. The fluorescence intensity of photo micrographs was measured by determining the mean pixel intensity using Image J software.

6.11. Amyloid- β induced paralysis assay

C. elegans strain CL4176 was maintained at 16 °C on *E. coli* OP50 bacterial lawn. Synchronized L1 larvae were transferred to NGM plates previously loaded with 50 μM concentrations of complexes **1**–**4** and 0.3% DMSO as solvent control and incubated for 50 h at 16 °C. The worms were transferred from 16 °C to 25 °C to initiate the Aβ induced paralysis and then the paralysis was scored at every 2 h intervals. The worms were decided as paralyzed based on the failure of the worms to move their body after gentle repeated prodding with a platinum wire. This test was terminated until the last worms become paralyzed. This experiment was performed on at least three independent biological replicates.

Acknowledgments

The author **G. D.** sincerely acknowledges Bharathiar University for University Research Fellowship No: C2/1531/2013 Dated (26.09.2013). The author P.K. gratefully acknowledges Department of Science and Technology (DST-SERB), New Delhi, India (No. SB/FT/CS-056-/2014 dated 12.08.2015) for the financial support and Dr. MuthuTamizh, Assistant Professor, Department of Chemistry, SRM University is acknowledged for his help in NMR studies. The authors acknowledge for some strains that were provided by the CGC, USA which is funded by NIH Office of Research Infrastructure Programs (P40 OD010440).

Appendix A. Supplementary data

Supplementary data related to this article can be found at http://dx.doi.org/10.1016/j.jorganchem.2017.03.023.

References

[1] S. Salvioli, E. Sikora, E.L. Cooper, C. Franceschi, Evid. Based Complement. Altern. Med. 4 (2007) 181–190.
[2] E. Sikora, A. Bielak-Zmijewska, G. Mosieniak, K. Piwocka, Curr. Pharm. Des. 16 (2010) 884–892.
[3] E. Sikora, G. Scapagnini, M. Barbagallo, Immun. Aging 7 (2010) 1.
[4] D. Harman, J. Gerontology 11 (1956) 298–300.
[5] J.M. McCord, I. Fridovich, J. Biol. Chem. 244 (1969) 6049–6055.
[6] G. Barja, Trends Neurosci. 27 (2004) 595–600.
[7] I. Fridovich, Ann. N. Y. Acad. Sci. 893 (1999) 13–18.
[8] M.K. Brown, J.L. Evans, Y. Luo, Pharmacol. Biochem. Behav. 85 (2006) 620–628.
[9] M.A. Wilson, B. Shukitt-Hale, W. Kalt, D.K. Ingram, J.A. Joseph, C.A. Wolkow, Aging Cell 5 (2006) 59–68.
[10] G. Gruunz, K. Haas, S. Soukup, M. Klingenspor, S.E. Kulling, H. Daniel, B. Spanier, Mech. Aging Dev. 133 (1) (2012) 1–10.
[11] R.A. Mekheimer, A.A.R. Sayed, E. Ahmed, J. Med. Chem. 55 (2012) 4169–4177.
[12] B.J. Goldstein, K. Mahadev, X. Wu, Diabetes 54 (2005) 311–321.
[13] V. Chavez, A. Mohri-Shiomi, A. Maadani, L.A. Vega, D.A. Garsin, Genetics 176 (2007) 1567–1577.
[14] D.J. Selkoe, Physiol. Rev. 81 (2001) 741–766.
[15] B. Torok, S. Dasgupta, M. Torok, Curr. Bioact. Compd. 4 (2008) 159–174.
[16] K.J. Barnham, V.B. Kenche, G.D. Ciccotosto, D.P. Smith, D.J. Tew, X. Liu, K. Perez, G.A. Cranston, T.J. Johanssen, I. Volitakis, A.I. Bush, C.L. Masters, A.R. White, J.P. Smith, R.A. Cherny, R. Cappai, Proc. Natl. Acad. Sci. U.S.A. 105 (2008) 6813–6818.
[17] D.M. Martin, N.D. Chasteen, J.K. Grady, Biochim. Biophys. Acta 1076 (1991) 252–258.
[18] D. Valensin, P. Anzini, E. Gaggelli, N. Gaggelli, G. Tamasi, R. Cini, C. Gabbiani, E. Michelucci, L. Messori, H. Kozlowski, G. Valensin, Inorg. Chem. 49 (2010) 4720–4722.
[19] L. Messori, M. Camarri, T. Ferraro, C. Gabbiani, D. Franceschini, ACS Med. Chem. Lett. 4 (2013) 329–332.
[20] P. Faller, C. Hureau, O. Berthoumieu, Inorg. Chem. 52 (2013) 12193–12206.
[21] M.G. Savelieff, S. Lee, Y. Liu, M.H. Lim, ACS Chem. Biol. 8 (2013) 856–865.
[22] A.H.J. Oliver, A.D. Daniel, L.C. Damien, A.K. Konstantinos, J.B. David, R. Ute, Metallomics 7 (2015) 29–38.
[23] I. Antoshechkin, P.W. Sternberg, Nat. Rev. Genet. 8 (2007) 518–532.
[24] T. Kaletta, M.O. Hengartner, Nat. Rev. Drug Discov. 5 (2006) 387–398.
[25] National Research Council (NRC) Scientific Frontiers in Developmental Toxicology and Risk Assessment vol. 296, The National Academies Press, Washington, DC, 2000.
[26] S. Medicia, M. Peanaa, V.M. Nurchib, J.I. Lachowiczb, G. Crisponib, M.A. Zoroddu, Coord. Chem. Rev. 284 (2015) 329–350.
[27] R. Archaryya, F. Basuli, S.M. Peng, G.H. Lee, L.R. Falvello, S. Bhattacharya, Inorg. Chem. 45 (2006) 1252–1259.
[28] R. Prabhakaran, R. Karvembu, T. Hashimoto, K. Shimizu, K. Natarajan, Inorg. Chim. Acta 358 (2005) 2093–2096.
[29] R. Prabhakaran, S.V. Renukadevi, R. Karvembu, R. Huang, J. Mautz, G. Huttner, R. Subashkumar, K. Natarajan, Eur. J. Med. Chem. 43 (2008) 268–273.
[30] P. Kalaivani, R. Prabhakaran, M.V. Kaveri, R. Huang, R.J. Staples, K. Natarajan, Inorg. Chim. Acta 405 (2013) 415–426.
[31] Y.P. Tian, C.Y. Duan, Z.L. Lu, X.Z. You, Polyhedron 15 (1996) 2263–2271.
[32] S. Dey, V.K. Jain, A. Kwoedler, W. Kaim, Ind. J. Chem. 42 A (2003) 2344–2351.
[33] D.M. Boghaei, S. Mohebi, J. Chem. Res. 6 (2001) 224–226.
[34] P. Govindaswamy, Y.A. Mozharivskyj, M.R. Kollipara, Polyhedron 23 (2004) 1567–1572.
[35] F. Basuli, M. Ruf, C.G. Pierpont, S. Bhattacharya, Inorg. Chem. 37 (1998) 6113–6116.
[36] P. Kalaivani, R. Prabhakaran, P. Poornima, F. Dallemer, K. Vijayalakshmi, V. Vijaya Padma, K. Natarajan, Organometallics 31 (2012) 8323–8332.
[37] R. Prabhakaran, S. Anantharaman, M. Thilagavathi, M.V. Kaveri, P. Kalaivani, R. Karvembu, N. Dharmaraj, H. Bertagnolli, F. Dallemer, K. Natarajan, Spectrochim. Acta. Part A 78 (2011) 844–853.
[38] D.R. Richardson, D.S. Kalinowski, V. Richardson, P.C. Sharpe, D.B. Lovejoy, M. Islam, P.V. Bernhardt, J. Med. Chem. 52 (2009) 1459–1470.
[39] (a) F. Basuli, S.M. Peng, S. Bhattacharya, Inorg. Chem. 36 (1997) 5645–5647; (b) F. Basuli, S.M. Peng, S. Bhattacharya, Inorg. Chem. 39 (2000) 1120–1127; (c) F. Basuli, S.M. Peng, S. Bhattacharya, Inorg. Chem. 40 (2001) 1126–1133.
[40] S. Ramakrishnan, E. Suresh, A. Riyasdeen, M.A. Akbarsha, M. Palaniandavar, Dalton Trans. 40 (2011) 3245–3256.
[41] A.K. Parta, S. Dhar, M. Nethaji, A.R. Chakravarty, Dalton Trans. (2005) 896–902.
[42] H.Y. Liu, Z.H. Xu, X.H. Liu, Chem. Pharm. Bull. 57 (2009) 1237–1242.
[43] A. Sulkowska, J. Mol. Struct. 614 (2002) 227–232.
[44] Y.Q. Wang, H.M. Zhang, G.C. Zhang, W.H. Tao, S.H. Tang, J. Lumin 126 (2007) 211–218.
[45] M. Jiang, M.X. Xie, D. Zheng, Y. Liu, X.Y. Li, X. Chen, J. Mol. Struct. 692 (2004) 71–80.
[46] N. Wang, L. Ye, B.Q. Zhao, J.X. Yu, J. Med. Biol. Res. 41 (2008) 589–595.
[47] C. Kontogiorgis, D. Hadjipavlou-Litina, J. Enzyme Inhib. Med. Chem. 18 (2003) 63–69.
[48] R. Yu, S. Mandlekar, A.T. Kong, Mol. Pharmacol. 58 (2000) 431–437.
[49] J. Asthana, A. Panta, D. Yadav, R.K. Lal, M.M. Gupta, R. Pandey, Industrial Crops Prod. 76 (2015) 1086–1093.
[50] R.V. Jacques, Biochem. J. 292 (1993) 605–608.
[51] J. Blum, I. Fridovich, Arch. Biochem. Biophys. 222 (1983) 35–43.
[52] D.K. Kim, H. Jeon, D.S. Cha, J. Funct. Foods 7 (2014) 630–640.
[53] S. Abbas, M. Wink, Planta. Med. 75 (2009) 216–221.
[54] N. Ishii, M. Fujii, P.S. Hartman, M. Tsuda, K. Yasuda, N. Senoo-Matsuda, S. Yanase, D. Ayusawa, K. Suzuki, Nature 394 (1998) 694–697.
[55] N. Senoo-Matsuda, K. Yasuda, M. Tsuda, T. Ohkubo, S. Yoshimura, H. Nakazawa, P.S. Hartman, N. Ishii, J. Biol. Chem. 276 (2001) 41553–41558.
[56] D. Gems, A.J. Sutton, M.L. Sundermeyer, P.S. Albert, K.V. King, M.L. Edgley, Genetics 150 (1998) 129–155.
[57] T. Heidler, K. Hartwig, H. Daniel, U. Wenzel, Biogerontology 11 (2010) 183–195.
[58] A. Kampkotter, C. Gombitang Nkwonkam, R.F. Zurawski, C. Timpel, Y. Chovolou, Arch. Toxicol. 81 (2007) 849–858.
[59] T. Furuyama, T. Nakazawa, I. Nakano, N. Mori, Biochem. J. 349 (2000) 629–634.
[60] C.D. Link, A. Taft, V. Kapulkin, K. Duke, S. Kim, Q. Fei, D.E. Wood, B.G. Sahagan, Neurobiol. Aging 24 (2003) 397–413.
[61] D.A. Butterfield, Curr. Med. Chem. 10 (2003) 2651–2659.
[62] K. Ono, K. Hasegawa, H. Naiki, M. Yamada, Neurochem. Int. 48 (2006) 275–285.
[63] S. Gottlieb, G. Ruvkun, Genetics 137 (1994) 107–120.
[64] C.T. Murphy, S.A. Mc Carroll, C.I. Bargmann, A. Fraser, R.S. Kamath, J. Ahringer, H. Li, C. Kenyon, Nature 424 (2003) 277–283.
[65] A.I. Vogel, Text Book of Practical Organic Chemistry, vth ed., Longman London, 1989, p. 268.
[66] P. Kalaivani, R. Prabhakaran, F. Dallemer, P. Poornima, E. Vaishnavi, E. Ramachandran, V. Vijaya Padma, R. Renganathan, K. Natarajan, Metallomics 4 (2012) 101–113.
[67] M.I. Bruce, N.J. Windsor, Aust. J. Chem. 30 (1977) 1601–1604.
[68] R.H. Blessing, An empirical correction for absorption anisotropy, ActaCrystallo. Sect. A 51 (1995) 33–38.
[69] G.M. Sheldrick, SHELXTL Version 5.1, An Integrated System for Solving, Refining and Displaying Crystal Structures from Diffraction Data, Siemens Analytical X-ray Instruments, Madison, WI, 1990.
[70] G.M. Sheldrick, Shelxl-97, A Program for Crystal Structure Refinement Release 97-2, Institut fur AnorganischeChemie der Universitat Gottingen, Tammanstrasse 4, D-3400, Gottingen, Germany, (1998).
[71] A. Braca, N.D. Tommasi, L.D. Bari, C. Pizza, M. Politi, I. Morelli, J. Nat. Prod. 64 (2001) 892–895.
[72] S. Brenner, Genetics 77 (1974) 71–94.